Nanoscale

Electronic supplementary information

Hidden energy levels? Carrier transport ability into $CdS/CdS_{1-x}Se_x$ quantum dot solar cells impacted by Cd-Cd level formation

Andrés. F. Gualdrón-Reyes,[a,b] Angel M. Meléndez,[b] Juan Tirado,[c] Mario Alejandro Mejía-Escobar,[c] Franklin Jaramillo,[c] and Martha E. Niño-Gómez*[a,b]

[a]*Centro de Investigaciones en Catálisis (CICAT), Universidad Industrial de Santander, Sede UIS Guatiguará, Piedecuesta, Santander, Colombia. C.P. 681011.*

[b]*Centro de Investigación Científica y Tecnológica en Materiales y Nanociencias (CMN), Universidad Industrial de Santander, Piedecuesta, Santander, Colombia. C.P. 681011.*

[c]*Centro de Investigación, Innovación, y Desarrollo de Materiales (CIDEMAT), Universidad de Antioquia, Calle 70 No. 52-21, Medellín, Colombia. C.P. 050010.*

*Corresponding Author: mobile: +57 3156487149

Email address: marthan@uis.edu.co (M.E. Niño-Gómez)

1. Deposition of cadmium chalcogenides on BNF-TNT

Fig. S1a-f shows typical FESEM top view and cross section images of BNF-TNT, 4-CdS and 4-CdS-5-$CdS_{1-x}Se_x$ photoanodes. Bare BNF-TNT are compact displaying a pore diameter distribution around 117.3 ± 1.7 nm and wall thickness of 18.5 ± 2.5 nm. Tubes are vertically aligned, showing an average length of 16.6 ± 1.3 µm. After sensitization, it could be observed the sealing of interspace tube and the presence of nanoparticles along the tubular structure and the top of pores. The average pore size and wall thickness were decreased to be 107.1 ± 2.5 nm and 35.0 ± 4.1 nm for the BNF-4-CdS composite, respectively, while for the BNF-4-CdS-5-$CdS_{1-x}Se_x$, its corresponding values were 96.3 ± 5.9 nm and 60.5 ± 9.1 nm. This indicates that large pores facilitated the penetration of the Cd^{2+}, S^{2-} and Se^{2-} alcoholic SILAR precursors into the inner and outer side of BNF-TNT.[1,2] A well-covered surface in each composite was obtained, which is beneficial to enhance their light harvesting capability.

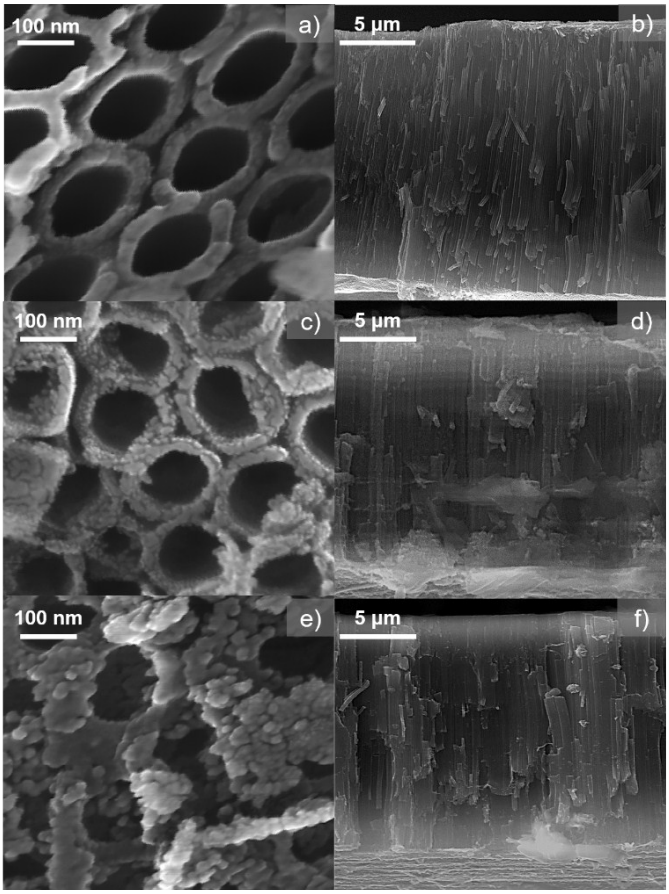

Fig. S1. FESEM images of top-view and cross-section of a,b) BNF-TNT, c,d) BNF-4-CdS and e,f) BNF-4-CdS-5-$CdS_{1-x}Se_x$ composite photoanodes.

2. Chemical environment of BNF-TNT

HR-XPS N 2p spectrum displays three peaks at 397.6, 399.7 and 402.8 eV. These peaks were attributed to the substitutional (N-Ti-N and N-Ti-O bonds) and interstitial N (N-O-Ti bonds) or NO_x adsorbed on BNF-TNT, respectively.[3,4] F 1s peak was also showed at 684.1 eV, associated to substitutional F into TiO_2.[1,3] B 1s spectrum provided a unique peak at 190.5 eV, ascribed to the interstitial boron (B-O-Ti bonds) into TiO_2.[1,5] The incorporation of substitutional F/interstitial B affected the chemical species of Ti, observed in the Ti 2p spectrum. Peaks at 458 and 463.6 eV corresponded to Ti^{4+} species from TiO_2, while peaks achieved at 455.8 and 461.2 eV were attributed to Ti^{3+} species.[1,3,5] A doublet observed at 460 and 465.3 eV was ascribed to Ti-F, according with the assigned contribution in the F 1s spectrum.[6]

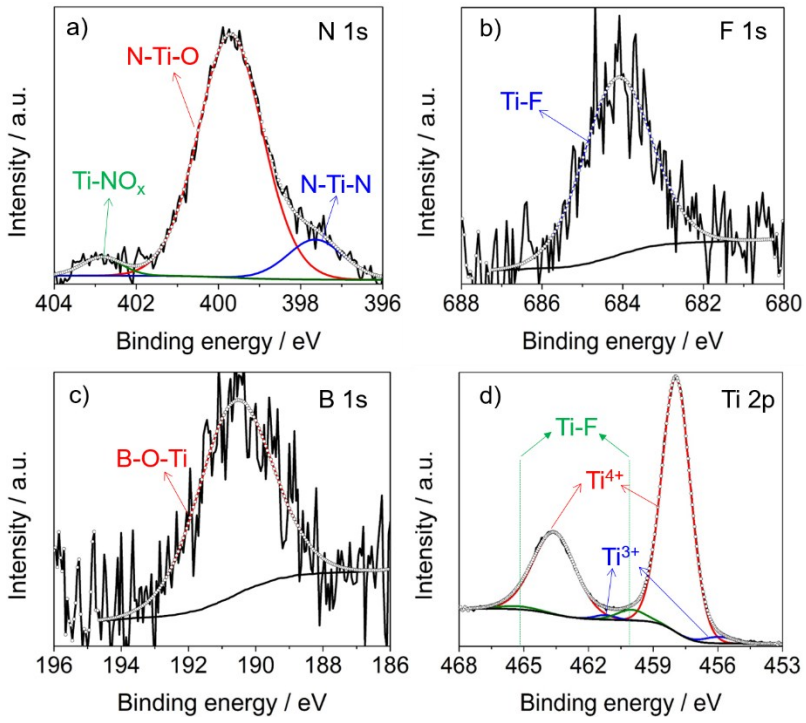

Fig. S2. High-resolution XPS a) N 1s, b) F 1s, c) B 1s and d) Ti 2p of the BNF-TNT based photoanodes.[7]

3. Stability of CuS/FTO and Cu_2S/Cu based cathodes used in 4-CdS-QDSSCs

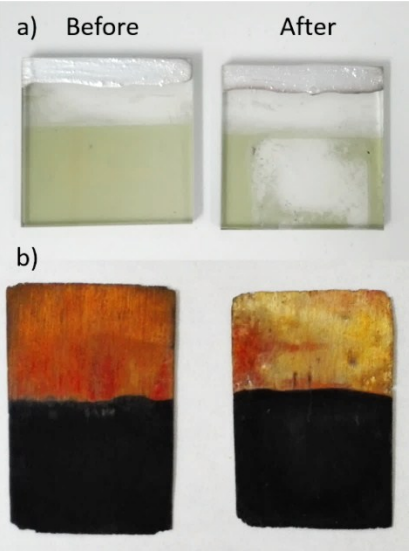

Fig. S3. Photographs of a) CuS/FTO and b) Cu_2S/Cu based cathodes before and after phovoltaic measurements.

4. Electrochemical Impedance spectra of Y-CdS-sensitized BNF-TNT photoanodes

The carrier transport capability of individual BNF-Y-CdS varying the load of CdS QD deposited by SILAR method was studied by EIS under visible illumination (Fig. S4). To understand the interfacial process occurring in the composites, Nyquist plots obtained for each material were fitted with a serie resistance and two Randles-type circuits connected in serie. This rearrangement was associated to the presence of two interfaces into BNF-Y-CdS composites. EIS parameters obtained from the fitted plots are shown in Table S1. R_s was the ITO resistance/contact from the external circuit of cell. R_1 and CPE_1 were ascribed to electron transport ability and capacitance in the ITO/BNF-TNT/CdS interfaces, while R_2 and CPE_2 were associated to interfacial carrier transfer resistance and its corresponding capacitance in the BNF-CdS/electrolyte interface.[8-10]

It was noteworthy from Table S1 that R_1 and R_2 were diminished to increase the SILAR cycles until 4. The decrease of the resistance values in each interface is the evidence of facilitated carrier transport from the electrolyte to CdS QD, which can oxidize the S^{2-}/SO_3^{2-} redox couple in the photoanode/electrolyte interface and avoid its photodecomposition. The accumulation of the sulfur species on the BNF-4-CdS surface could be observed to obtain a higher CPE_2 than those the others photoanodes. It agrees with the increase of signals of adsorbed species seen in photopotential measurements. Then, accumulated photoelectrons in the CdS are injected via CB to BNF-TNT, mediated by a suitable II-type heterojunction.[11,12] The enhancement of the conducting properties in the composite was noted to evidence the lowest CPE_1, associated to an efficient charge carrier separation into the material. Conversely, after 5-CdSe and 6-CdSe sensitization, R_1 and R_2 values were increased while the CPE_1 and CPE_2 showed an increase/decrease behaviour. The charge carrier accumulation in the BNF-5-CdS and BNF-6-CdS interface is the main indication of electron injection suppressing into CB of BNF-TNT from CdS QD, where a high likelihood of charge carrier recombination can be achieved. Although the incorporation of Cd-Cd energy states increases the ability of CdS to capture lower-energy photons decreasing its E_g without shifting the CB edge,[13] an excess of Cd-Cd levels can act as recombination centers, blocking electron transfer in the composite.

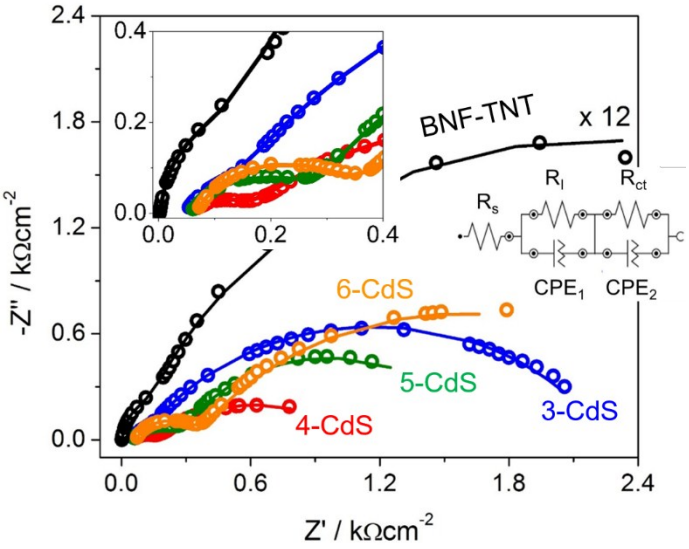

Fig. S4. Nyquist plots (10 kHz–0.01 Hz) of BNF-Y-CdS photoanodes in function of number of SILAR cycles (Y). Insets of Fig. S4 show the Nyquist semicircle at high frequencies and equivalent circuit after EIS spectra fitting. Electrolyte: 0.25 M Na_2S + 0.35 M Na_2SO_3 (pH 12), illumination source: halide lamp (60 $mWcm^{-2}$).

Table S1. Fitted EIS parameters of BNF-Y-CdS photoanodes.

Photoanode	Rs / Ωcm^{-2}	R_l / Ωcm^{-2}	R_{ct} / Ωcm^{-2}	CPE_1 / μFcm^{-2}	CPE_2 / μFcm^{-2}
Bare BNF-TNT	25	930	51485	36	49
BNF-3-CdS	48	342	2154	49	69
BNF-4-CdS	60	93	938	12	2310
BNF-5-CdS	57	220	1392	16	562
BNF-6-CdS	67	277	2487	35	792

5. Open-circuit potential of the BNF-4-CdS-5-$CdS_{1-x}Se_x$ photoanodes in function of the S/Se molar ratio

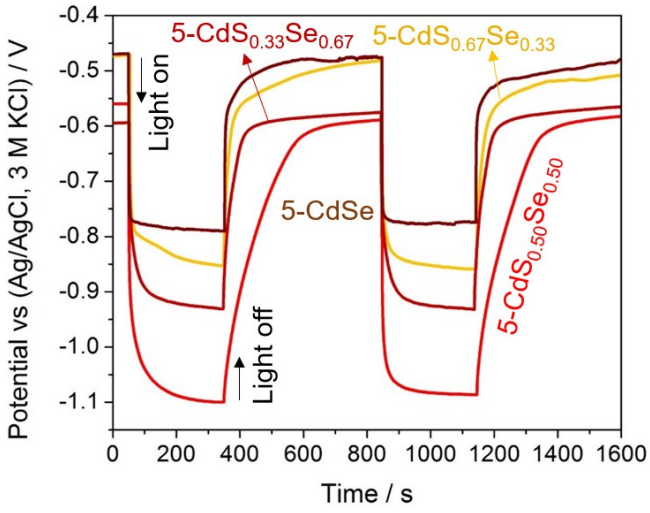

Fig. S5. Open circuit photopotential of the BNF-4-CdS-5-$CdS_{1-x}Se_x$ photoanodes in function of S/Se molar ratio into ternary alloy. Electrolyte: 0.25 M Na_2S + 0.35 M Na_2SO_3 (pH 12), illumination source: halide lamp (60 $mWcm^{-2}$).

6. Electrochemical Impedance spectra of $CdS_{1-x}Se_x$-sensitized BNF-4-CdS photoanodes

The 5-$CdS_{1-x}Se_x$ sensitization of BNF-4-CdS also caused changes in the conducting properties of the composites, which were individually studied by electrochemical impedance spectroscopy (EIS) through Nyquist plots (Fig. S6). Similar for the BNF-Y-CdS described above, two semicircles were obtained in the corresponding EIS spectra and fitted to a two Randles-type circuits connected in serie. R_s was associated to the connection between conducting glass substrate and the external circuit of the cell. R_1 and CPE_1 were ascribed to carrier transfer and accumulation processes in the BNF-TNT/CdS/$CdS_{1-x}Se_x$ interfaces, while R_2 and CPE_2 corresponded to electron transport ability in the CdS/$CdS_{1-x}Se_x$/electrolyte interface.[11,12] EIS parameters extracted from the respective Nyquist curves are displayed in Table S2, where showed a widely dependence on the S/Se molar ratio in the alloy. To decrease the S/Se molar ratio to 1.0, R_1, R_2 and CPE_1 were also decreased, indication of an efficient electron-hole pair separation into the $CdS_{1-x}Se_{x,}$ and electron transport from this sensitizer to BNF-TNT using the CdS as a "charge bridge". The II-type heterojunction in the CdS/$CdS_{1-x}Se_x$ interface promoted electron injection to CdS via CB, avoiding the charge recombination.[14]

A low electron mobility resistance increases the charge carrier lifetime in the composite, agreeing with a slow OCPD observed in photopotential measurements. More electrolyte species can renew the electrons in the $CdS_{1-x}Se_x$, increasing the CPE_2 value. For S/Se < 0.5, R_1, R_2 and CPE_1 were increased, while the CPE_2 value was decreased. Here, the electron accumulation mediated by I-type heterojunction promotes carrier recombination in the co-sensitizers interface, Thus, a low amount of sulfur species is accumulated in the $CdS_{1-x}Se_x$/electrolyte interface to inject electrons to the ternary alloy. Despite the unsuitable band alignment in the CdS/CdSe interface observed by the highest R_1 and CPE_1, the corresponding R_2 and CPE_2 values were lower than that composite with S/Se = 0.5. This suggested that CdSe could photogenerate charge carriers which were separated and injected to a Cd-Cd energy levels into CdS, renewing the electrons in CdSe by the electrolyte. However, the electrons promoted to the CB of CdS could returned to CdSe via CB, mediating electron recombination with oxidized sulfur species from S^{2-} /SO_3^{2-} redox couple.[11,15]

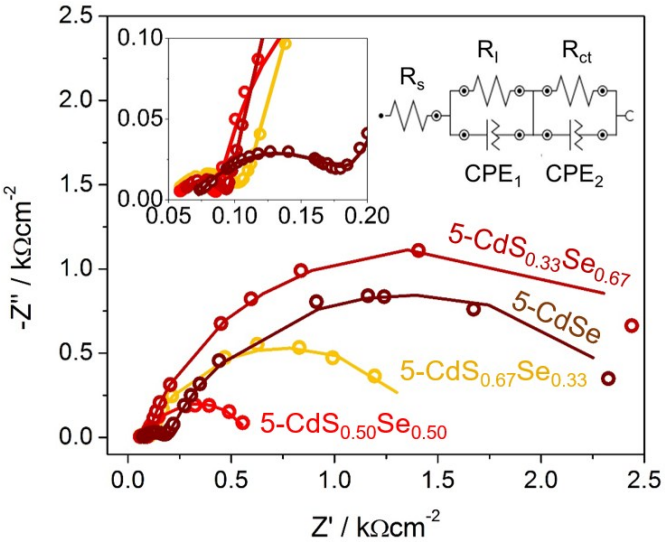

Fig. S6. Nyquist plots (20 kHz–0.01 Hz) of BNF-4-CdS-5-$CdS_{1-x}Se_x$ photoanodes in function of S/Se molar ratio into ternary alloy. Insets of Fig. S5 show the Nyquist semicircle at high frequencies and equivalent circuit after EIS spectra fitting. Electrolyte: 0.25 M Na_2S + 0.35 M Na_2SO_3 (pH 12), illumination source: halide lamp (60 $mWcm^{-2}$).

Table S2. Fitted EIS parameters of BNF-4-CdS-5-$CdS_{1-x}Se_x$ photoanodes.

Photoanode	Rs / Ωcm^{-2}	R_l / Ωcm^{-2}	R_{ct} / Ωcm^{-2}	CPE_1 / μFcm^{-2}	CPE_2 / μFcm^{-2}
5-$CdS_{0.67}Se_{0.33}$	51	59	1315	111	2008
5-$CdS_{0.50}Se_{0.50}$	64	31	575	40	3377
5-$CdS_{0.33}Se_{0.67}$	58	38	2771	47	1710
5-CdSe	94	132	2344	68	1042

7. Incident photon-to-current efficiency (IPCE) spectra of BNF-4-CdS and BNF-4-CdS-5-$CdS_{0.5}Se_{0.5}$ photoanodes

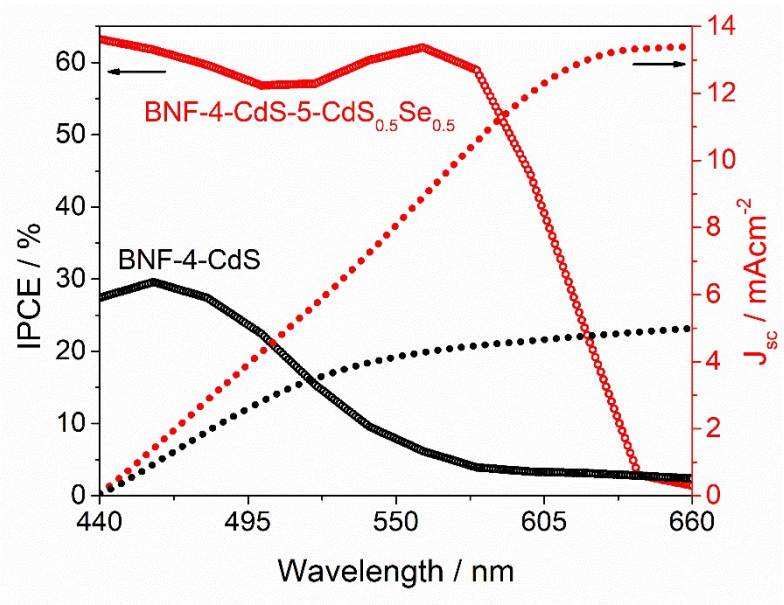

Fig. S7. IPCE spectra of BNF-4-CdS and BNF-4-CdS-5-$CdS_{1-x}Se_x$ photoanodes (S/Se molar ratio = 0.5).

8. Valence band edge (E_{VB}) determination in BNF-4-CdS-5-$CdS_{1-x}Se_x$ composites

By extrapolating to 0 eV the corresponding slopes in the XPS valence band spectra for the studied materials, the E_{VB} values were estimated to be (2.14, 0.84, 0.46, 0.44, 0.41, and 0.32) eV for BNF-TNT, BNF-4-CdS, BNF-4-CdS-5-$CdS_{1-x}Se_x$ (S/Se molar ratio = 2.0, 1.0 and 0.5) and 5-CdSe, respectively (Fig. S7). Their conduction band edges (E_{CB}) were calculated by using the equation (5), and converted to potential scale vs Ag/AgCl, 3 M KCl (+210 mV vs NHE) by equation (9) in the manuscript. Both the E_{CB} and E_{VB} were narrowed to increase the amount of added Se into ternary alloy, establishing a balance between light harvesting and band alignment in the formed CdS/$CdS_{1-x}Se_x$ heterostructure.

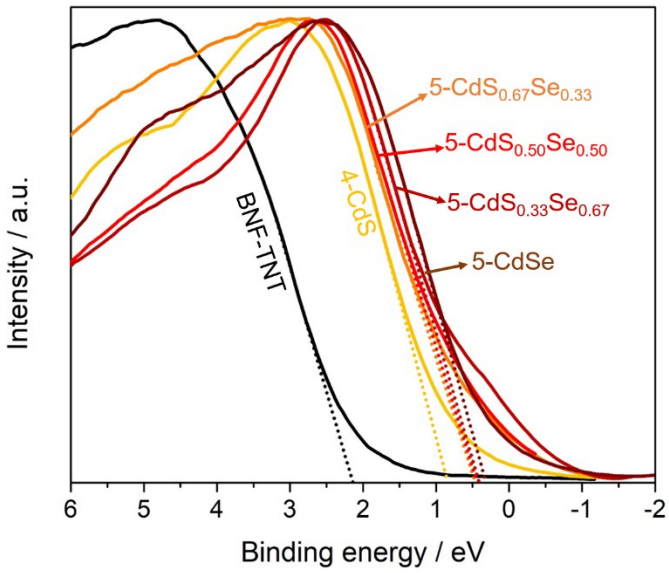

Fig. S8. Normalized XPS valence band spectra of BNF-TNT, BNF-4-CdS and BNF-4-CdS-5-$CdS_{1-x}Se_x$ photoanodes varying the S/Se molar ratio contained into ternary alloy.

Referencies

1. A. F. Gualdrón-Reyes, A. M Meléndez, M. A. Mejía-Escobar, F. Jaramillo and M. E. Niño-Gómez, *New. J. Chem.,* 2018, **42**, 14481.
2. H. Lee, M. Wang, P. Chen, D. R. Gamelin, S. M. Zakeeruddin, M. Grätzel and Md. K. Nazeeruddin, *Nano Lett.,* 2009, **9,** 4221.
3. L. J. Hoyos, D. F. Rivera, A. F. Gualdrón-Reyes, R. Ospina, J. Rodriguez-Pereira, J. L. Ropero-Vega and M. E. Niño-Gómez, *Appl. Surf. Sci.,* 2017, **423,** 917.
4. G. Yang, Z. Jiang, H. Shi, T. Xiao and Z. Yan, *J. Mater. Chem.,* 2010, **20,** 5301.
5. F. J. Mancilla, S. F. Rojas, A. F. Gualdrón-Reyes, M. I. Carreño-Lizcano, L. J. Duarte and M. E. Niño Gómez, *RSC Adv.,* 2016, **6,** 46668.
6. T. Sultana, G. L. Georgiev, G. Auner, G. Newaz, H. J. Herfurth and R. Patwa, *Appl. Surf, Sci.,* 2008, **255,** 2569.
7. A. F. Gualdrón-Reyes, A. Cárdenas-Arenas, C. A. Martínez, V. V. Kouznetsov and A. M. Meléndez, *J. Phys. Conf. Ser.,* 2017, **786,** 012044.
8. S. Majumder and B. R. Sankapal, *New J. Chem.,* 2017, **41,** 5808.
9. J. Yu, C. Gong, Z. Wu, Y. Wu, W. Xiao, Y. Su, L. Sun and C. Lin, *J. Mater. Chem. A,* 2015, **3,** 22218.
10. M. A. Mahadik, P. S. Shinde, M. Cho and J. S. Jang, *J. Mater. Chem. A,* 2015, **3,** 23597.
11. S. Naskar, F. Lübkemann, S. Hamid, A. Freytag, A. Wolf, J. Koch, I. Ivanova, H. Pfnür, D. Dorfs, D. W. Bahnemann, and Nadja C. Bigall*, Adv. Funct. Mater.,* 2017, 1604685.
12. P. Chang, H. Cheng, W. Li, L. Zhuo, L. He, Y. Yu and F. Zhao, *Phys. Chem. Chem. Phys.,* 2014, **16,** 16606.
13. H. Tong, N. Umezawa, J. Ye and T. Ohno, *Energy Environ. Sci.,* 2011, **4,** 1684.
14. Z. Li, L. Yu, Y. Liu and S. Sun, *Electrochim. Acta,* 2015, **153,** 200.
15. B. Zhang, J. Zheng, X. Li, Y. Fang, L.-W. Wang, Y. Lin and F. Pan, *Chem. Commun.,* 2016, **52,** 5706.